

Frascati, March 27, 1996

Note: **G-38**

**ION TRAPPING EFFECT AND CLEARING IN THE
DAΦNE MAIN ELECTRON RING**

C. Vaccarezza

To be submitted to Physical Review E.

INTRODUCTION	1
I. TUNE SHIFT AND NEUTRALISATION FACTOR	1
II. LINEAR THEORY	3
III. NON LINEAR THEORY	4
IV. POTENTIAL WELL CALCULATION.....	5
V. EQUATIONS OF THE ION MOTION IN PRESENCE OF AN ELECTRON BEAM	7
VI. DC ION CLEARING AND RF BEAM SHAKING	10
VII. ION MOTION TRACKING RESULTS.....	11
VIII. CONCLUSIONS	14
Appendix A	
“Calculation of the relevant parameters of the ion clearing system for the DAΦNE Electron Main Ring”	15
Appendix B	
“Solution of the Poisson equation with Dirichlet boundary conditions for a rectangular box of infinite length”	17

Appendix C	
“Solution of the Poisson Equation with Dirichlet b.c. for a circular box of infinite length”	19
Appendix D	
“Calculation of the Electric Field due to a Clearing Electrode for a rectangular box of infinite length”	21
Appendix E	
“Calculation of the Electric Field due to a Clearing electrode for a circular box of infinite length”	26
Appendix F.1	
“DAΦNE Electron Main Ring Layout”	28
Appendix F.2	
“DAΦNE First Bending Quadrant Layout”	29
Appendix G	
“Other results of tracking for trapped ions in the second Bending Quadrant of DAΦNE Electron Main ring”	30
REFERENCES	32

INTRODUCTION

The ionisation of the residual gas, present in the vacuum chamber, by the circulating electron beam is a well known phenomenon. Under certain conditions the ions can be trapped in the beam potential well and move on stable oscillating orbits inside the beam. This is the so called ‘‘Ion Trapping’’ effect that produces a general detriment of the electron beam performances such as tune-shift, spread, emittance blow-up, horizontal and vertical motion coupling, enhancements of elastic and inelastic collisions with the residual gas [2], and for an electron-positron storage ring an undesired loss of luminosity. To avoid these effects the ‘‘clearing’’ of the trapped ions has to be achieved by means of an ‘‘ion clearing’’ system which means the use of DC and RF electrodes or the set up of different operating conditions for the machine, (i.e. the asymmetrical filling of the electron bunches), which lead to the desired instability for the ion orbits.

In the first part of this report the general concepts of Ion Trapping are reported, providing the basic considerations for the DAΦNE ion clearing system. The Poisson equation for the potential well due to the electron beam has been solved in order to locate the minima of the function, and the suitable positions for the DC clearing electrodes.

The three-dimensional equations of motion have been written according to the lattice of the storage ring. The numerical integration of the ion motion equations has been performed with the help of the NAG FORTRAN Libraries and the results are shown for the two Bending Quadrants (BQ) of the DAΦNE Main Ring.

The DAΦNE clearing system is proposed.

I. TUNE SHIFT AND NEUTRALISATION FACTOR

The force on the electron beam in the electric field due to the ions trapped inside the beam is focusing for both horizontal and vertical planes [2]. The tune shift is given by:

$$\delta Q_{H,V} = \frac{1}{4\pi E} \int \beta_{H,V} \frac{\partial F_{x,y}}{\partial x,y} R d\theta, \quad (1)$$

where E is the electron energy, $\beta_{H,V}$ is the betatron function (horizontal or vertical), $F_{x,y}$ the force acting on the electrons, R the radius of the storage ring and θ the azimuthal angle.

Assuming that the longitudinal distribution of ions is uniform and the transverse distribution is a duplicate of that of the electron beam [3], the derivatives of the forces $\partial F_x / \partial x$ and $\partial F_y / \partial y$ are given by:

$$\begin{aligned} \frac{\partial F_x}{\partial x} &= \frac{N_j e^2}{\epsilon_0 \pi \sigma_H (\sigma_H + \sigma_V) C} = \frac{\eta I e}{\pi \epsilon_0 c \sigma_H (\sigma_H + \sigma_V)} \\ \frac{\partial F_y}{\partial y} &= \frac{N_j e^2}{\epsilon_0 \pi \sigma_V (\sigma_H + \sigma_V) C} = \frac{\eta I e}{\pi \epsilon_0 c \sigma_V (\sigma_H + \sigma_V)}, \end{aligned} \quad (2)$$

where N_j is the number of the ions, ε_0 the permittivity of the free space, σ_H and σ_V the horizontal and the vertical beam sizes respectively, C the circumference of the ring, e the electron charge, I the electron beam current, η the neutralisation factor, which is the ratio of the density of ions to electrons, and c is the velocity of light.

Assuming that the neutralisation factor η varies slowly over the entire circumference of the ring we can write[2]:

$$\begin{aligned}\delta Q_H &\equiv \frac{e}{4\pi^2 \varepsilon_0 c E} I \cdot \langle \eta \rangle \cdot \left\langle \frac{\sqrt{\beta_H}(1+K)}{\sqrt{\beta_H} + \sqrt{K\beta_V}} \right\rangle \frac{C}{\varepsilon_T} \\ \delta Q_V &\equiv \frac{e}{4\pi^2 \varepsilon_0 c E} I \cdot \langle \eta \rangle \cdot \left\langle \frac{\sqrt{\beta_V}(1+K)}{\sqrt{K}(\sqrt{\beta_H} + \sqrt{K\beta_V})} \right\rangle \frac{C}{\varepsilon_T},\end{aligned}\quad (3)$$

where K is the coefficient of coupling, ε_T is the emittance, and the symbol $\langle \rangle$ shows the average over the circumference of the ring.

The maximum tolerable value for $\delta Q_{H,V}$ sets the limit for $\langle \eta \rangle$, which can be written also as [3]:

$$\langle \eta \rangle \equiv \frac{\tau_{drift}}{\tau_{prod}}, \quad (4)$$

where τ_{drift} is the migration time of the ions and for τ_{prod} we have:

$$\frac{1}{\tau_{prod}} = c \cdot \sigma_p \cdot \bar{\rho}_g, \quad (5)$$

where c is the speed of light, σ_p the ion production cross section, and $\bar{\rho}_g$ the mean value of the residual gas density¹.

Once the limit for $\langle \eta \rangle$ is known we can obtain the maximum tolerable value for τ_{drift} which can be written also as:

$$\tau_{drift} = l / v_s \quad (6)$$

where v_s is the drift velocity of the ions and l represents the distance between the clearing electrodes locations.

¹ See Appendix A : "Calculations of the relevant parameters of the ion clearing system for the DAΦNE electron ring.

II. LINEAR THEORY

In the simplified linear model of ion trapping the interaction between ions and electron bunch is described with the help of the thin lenses approximation and the usual matrix formalism. The longitudinal velocity of the ions is always negligible compared with that of the relativistic stored electrons; moreover every variation of the drift ion velocity is also neglected. Let x and \dot{x} be the position and speed of the ion respectively. After the passage of an electron bunch the new position x_2 and speed \dot{x}_2 are obtained applying to the previous (x_1, \dot{x}_1) the linear operator M described by , [1]:

$$\begin{aligned} \begin{pmatrix} x_2 \\ \dot{x}_2 \end{pmatrix} &= M \begin{pmatrix} x_1 \\ \dot{x}_1 \end{pmatrix} \\ &= \begin{pmatrix} 1 & T_b \\ 0 & 1 \end{pmatrix} \begin{pmatrix} 1 & 0 \\ -\alpha & 1 \end{pmatrix} \begin{pmatrix} x_1 \\ \dot{x}_1 \end{pmatrix}, \end{aligned} \quad (7)$$

where T_b is the period of the electron bunches, and α is the linear kick parameter given by:

$$\alpha = \frac{N_e^{Tot} 4r_p c}{A 2p^2 \sigma_{H,V} (\sigma_H + \sigma_V)} \quad (8)$$

A = molecular number of the ion

r_p = classical proton radius

p = bunch number

c = speed of light

N_e^{Tot} =total number of circulating electrons

From the stability condition, imposed on the trace of the matrix, the critical ion mass A_c is obtained, above which the ion motion is stable:

$$A_c = \frac{N_e^{Tot} r_p C}{2p^2 \sigma_{H,V} (\sigma_H + \sigma_V)}. \quad (9)$$

C = circumference of the ring.

Another way to cope with the ion trapping effect is the asymmetrical filling of the electron bunches [4]. In this case we have:

$$\begin{pmatrix} x_2 \\ \dot{x}_2 \end{pmatrix} = \begin{pmatrix} 1 - \omega^2 \tau T_b & T_b \\ -\omega^2 \tau & 1 \end{pmatrix}^p \begin{pmatrix} 1 & T_b \cdot (h - p) \\ 0 & 1 \end{pmatrix} \begin{pmatrix} x_1 \\ \dot{x}_1 \end{pmatrix}, \quad (10)$$

where h is the harmonic number and p is the number of consecutively filled bunches.

The stability condition can be found numerically. Plotting the value of the matrix trace versus $1/A_i$ we obtain stability and instability bands for the ions, depending on the machine parameters, the current value I and the filling factor p , (see Fig. 1).

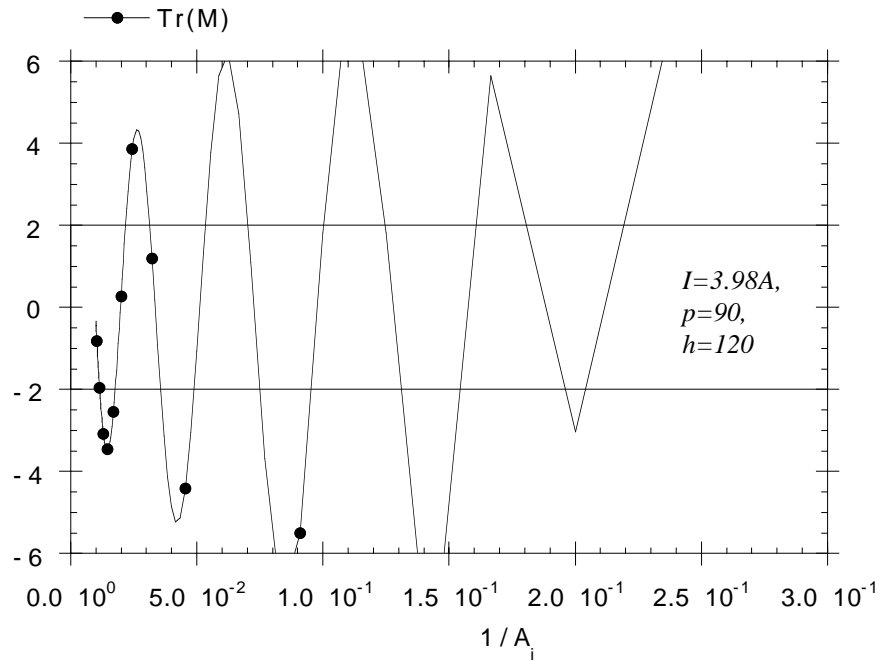


Figure 1. The trace of the motion matrix M is shown as a function of the reciprocal of the atomic mass number for a given beam size and current.

III. NON LINEAR THEORY

The electric field due to a Gaussian distribution of electric charge in both directions of the x-y plane can be written [5]:

$$\begin{pmatrix} E_x \\ E_y \end{pmatrix} = \begin{pmatrix} \text{Im}(Z) \\ \text{Re}(Z) \end{pmatrix} \quad \text{where:}$$

$$Z = A \cdot \left[w \left(\frac{x + iy}{\sqrt{2(\sigma_x^2 - \sigma_y^2)}} \right) - e^{-\left(\frac{x^2}{2\sigma_x^2} + \frac{y^2}{2\sigma_y^2} \right)} \cdot w \left(\frac{x \frac{\sigma_y}{\sigma_x} + iy \frac{\sigma_x}{\sigma_y}}{\sqrt{2(\sigma_x^2 - \sigma_y^2)}} \right) \right] \quad (12)$$

$$A = \frac{Ne}{2\epsilon_0 \sqrt{2\pi(\sigma_x^2 - \sigma_y^2)}}, \quad w(z) = e^{-z^2} \left[1 + \frac{2i}{\pi} \int_0^z e^{-\xi^2} d\xi \right].$$

In Fig. 2. E_y/Ne is plotted vs. the y/σ_x ratio for different values of the coupling factor k .

The linear behaviour actually lies only in the first one sigma range. As a consequence the strength of the electric field exerted on the ions strictly depends on their positions with the respect to the centre of the bunch.

For this reason it's better to track the motion of the residual ions instead to look for general statements that could oversimplify the problem.

Furthermore a three-dimensional analysis is needed to get a reliable description of the trapped ions motion.

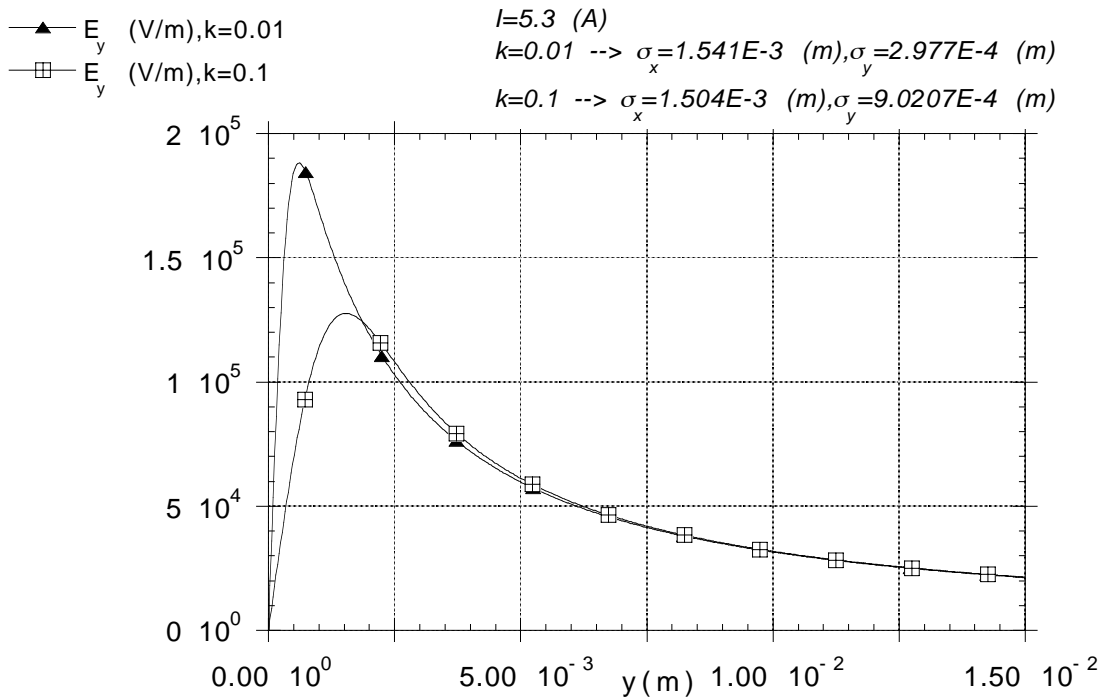
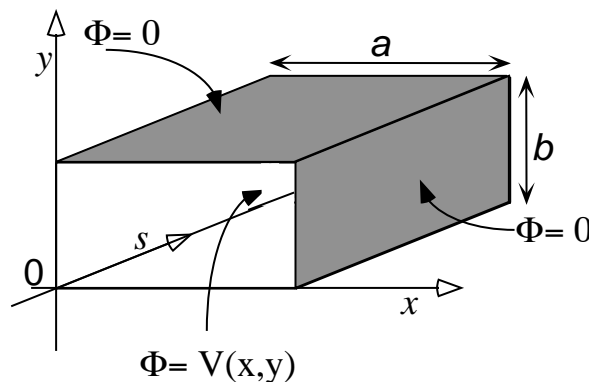


Figure 2. The vertical component of the electric field due to a Gaussian distribution of charge in both directions of the x-y plane, and a longitudinal linear density $\lambda = N_e^{Tot} \cdot e/C$, is plotted vs. the vertical co-ordinate. Two values of the coupling factor k have been considered.

IV. POTENTIAL WELL CALCULATION

In order to have a good scenario of the boundary conditions for the ion trapping effect the calculation of the potential well due to an electron beam has been carried out for a storage ring with a rectangular vacuum chamber .



In the continuous beam model we can consider an uniform electron distribution along the longitudinal co-ordinate s , and replace the time-dependent function with its average with respect to time. Finally we can write for the electron density $\rho(x,y)$:

$$\rho(x,y) = \frac{\lambda}{2\pi\sigma_x\sigma_y} \cdot e^{-\left(\frac{(x-X_c)^2}{2\sigma_x^2} + \frac{(y-Y_c)^2}{2\sigma_y^2}\right)}, \quad (12)$$

with $\lambda = \frac{N_e^{Tot} \cdot e}{C}$ = linear charge density and:

- x,y = horizontal and vertical transverse co-ordinates
- s = longitudinal co-ordinate of the motion of ions and electrons
- N_e^{Tot} = total number of electrons
- C = total circumference of the ring
- σ_x, σ_y = standard deviations of the electron distribution
- X_c, Y_c = beam centre transverse co-ordinates.

For the potential $\Phi(V)$ due to the presence of the electron distribution inside a rectangular vacuum chamber of infinite length we have²:

$$\begin{cases} \nabla^2 \Phi = -4\pi\rho & \text{inside the vacuum chamber} \\ \Phi = 0 & \text{on the chamber walls (i.e. Dirichlet b.c.)} \end{cases} \quad (13)$$

The solution can be found from the Green's function which satisfies:

$$\nabla'^2 G(\bar{x}, \bar{x}') = -4\pi\delta(\bar{x}, \bar{x}'). \quad (14)$$

Thus:

$$\begin{aligned} \Phi(\bar{x}) = & \int_V \rho(\bar{x}') G(\bar{x}, \bar{x}') d^3x' + \\ & + \frac{1}{4\pi} \oint_S \left[G(\bar{x}, \bar{x}') \frac{\partial \Phi}{\partial n'} - \Phi(\bar{x}') \frac{\partial G(\bar{x}, \bar{x}')}{\partial n'} \right] da'. \end{aligned} \quad (15)$$

The solution for our case is³:

$$\begin{aligned} \Phi(x,y) = & \lambda \frac{16}{\pi ab} \sum_{n,m} \frac{\sin\left(\frac{n\pi x}{a}\right) \sin\left(\frac{n\pi X_c}{a}\right) \sin\left(\frac{m\pi y}{b}\right) \sin\left(\frac{m\pi Y_c}{b}\right)}{\frac{n^2}{a^2} + \frac{m^2}{b^2}} \cdot \\ & \cdot \exp\left[-\left(\frac{\pi^2 n^2 \sigma_x^2}{2a^2} + \frac{\pi^2 m^2 \sigma_y^2}{2b^2}\right)\right], \end{aligned} \quad (16)$$

² C.G.S. units.

³ See Appendix B : "Solution of the Poisson equation with *Dirichlet boundary conditions* for a rectangular box of infinite length".

where a and b are the dimensions of the vacuum chamber cross-section. Strictly speaking, eq. (17) should give Φ as a function of (x,y) only. In practice, we have an implicit dependence on s through the variation of $X_c, Y_c, \sigma_x, \sigma_y$ along the vacuum chamber. This does not affect the validity of eq. (17), since the variation of $X_c, Y_c, \sigma_x, \sigma_y$ in s is slow with respect to the other relevant scale lengths of the problem. The results for the DAΦNE electron ring are shown in Fig. 3 for two values of the coupling factor k .

It is evident that the potential Φ depends on the longitudinal co-ordinate s through the variation of the beam size, the beam centre co-ordinates and the dimensions of the vacuum chamber cross sections. This is the reason why abrupt cross section variations can provide potential barriers for the longitudinal drift motion of the trapped ions. Therefore the balancing effects of the eventual tapering, designed to connect different cross sections of the beam vacuum chamber, have to be taken into account to well estimate the relevance of this type of barriers.

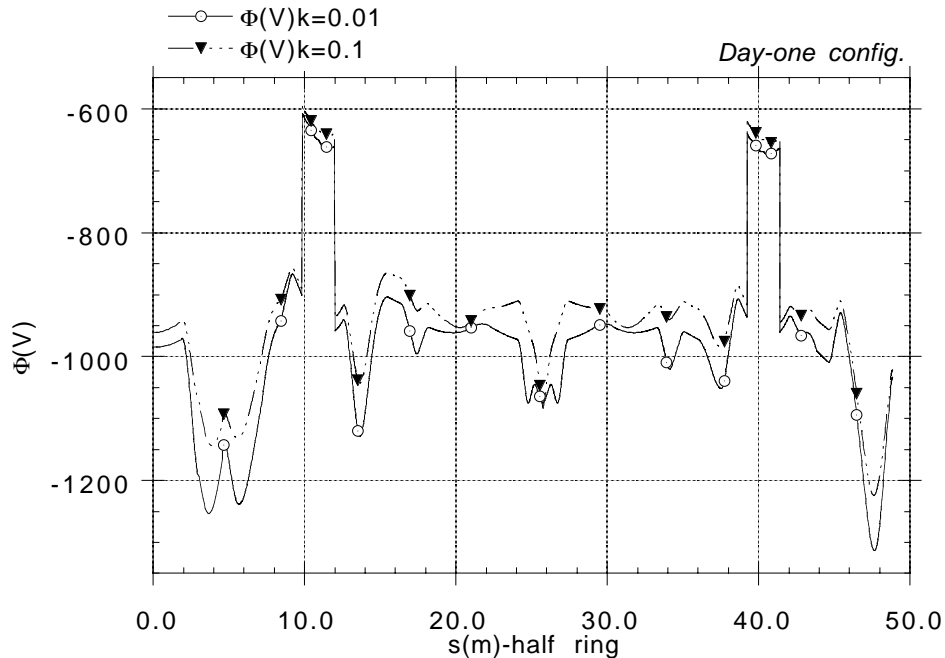


Figure 3. In this figure the potential well $\Phi(X_c, Y_c, s)$ is plotted vs. the longitudinal co-ordinate of half DAΦNE Main Ring, for two operating values of the coupling coefficient k , (X_c, Y_c are the beam centre co-ordinates). A rectangular vacuum chamber cross section has been considered; the two abrupt variations of the potential correspond to variations of the vacuum chamber cross section close to the Wiggler locations. The actual existing tapering is very smooth and calculation have been carried out to estimate its weight on the potential well behaviour. The effect of the tapering turned out to be very small comparing with the $\partial\Phi/\partial s$ induced by the local variations of the beam dimensions.

V. EQUATIONS OF THE ION MOTION IN PRESENCE OF AN ELECTRON BEAM

The analysis of the residual ion motion in a storage ring can be divided into three parts:

- a) free space(with no lattice elements)
- b) dipole section
- c) oscillating magnetic field section.

The equations of ion motion in the free space in presence of an electron beam are:

$$\begin{aligned}\ddot{x} &= -\frac{q}{M_i} E_x(x, y, s), \\ \ddot{y} &= -\frac{q}{M_i} E_y(x, y, s), \\ \ddot{s} &= -\frac{q}{M_i} E_s(x, y, s).\end{aligned}\tag{17}$$

Here s represents the longitudinal co-ordinate along the ring for familiarity with the usual machine physics representation.

E_x and E_y are the transverse components of the non-linear electric field due to a beam with Gaussian distribution in both directions, (see par. **III**). The longitudinal component $E_s(x, y, s)$ is obtained by:

$$E_s(x, y, s) = \frac{\Phi(x, y, \hat{s} + \Delta\hat{s}) - \Phi(x, y, \hat{s})}{\Delta\hat{s}},\tag{18}$$

where $\Phi(x, y, \hat{s})$ is a vector with the values of the potential well due to a linear distribution of the beam charge at discrete positions $\hat{s} = s_j$, $j = 1, 2, \dots, m$ along the ring circumference, (see par. **IV**), and \hat{s} is the discrete longitudinal variable closest to the s actual value. This is because the calculation of the series for the potential Φ is fast enough as stand-alone code but the series evaluation is too long to be used inside a numerical code for integration of differential equations. Moreover the expression adopted for $\Phi(x, y, \hat{s})$ is:

$$\Phi(x, y, s) = \Phi(X_0, Y_0, \hat{s}) - \left\{ \int_{X_0}^x E_x(x', Y_0) dx' + \int_{Y_0}^y E_y(x, y') dy' \right\},\tag{21}$$

where X_0, Y_0 are the beam centre co-ordinates and $E_{x,y}$ is the horizontal(vertical) component of the electric field due to the beam. This is because, again, it's faster to evaluate the two integrals of the right hand side of (20), representing the difference in the potential value from the beam centre position, than carrying out the summation over the series expansion at each step of the integration code.

The time dependence of the electric field of the beam due to its bunch structure has been taken into account turning on and off the charge density ρ according to the time distribution:

$$\rho = \rho_0 e^{-(t-t_0)^2/2\sigma_t^2}\tag{22}$$

where:

$$\begin{aligned}
 n &= \left[\frac{t}{t_0} \right], & C &= \text{ring circumference,} \\
 t_0 &= \frac{C}{c \cdot h}, & h &= \text{harmonic number,} \\
 \sigma_t &= \frac{\sigma_s}{c}, & p &= \text{\# of cons. filled bunches,} \\
 & & j &= \text{\# of machine turns,}
 \end{aligned}$$

and:

$$\begin{cases} \rho = \rho(t, n) & \text{for } n \leq p + j \cdot h \\ \rho = 0 & \text{elsewhere} \end{cases} \quad (21)$$

In presence of a static magnetic field, i.e. dipole section the (18) become:

$$\begin{aligned}
 \ddot{x} &= -\frac{q}{M_i} E_x - \frac{q}{M_i} \dot{s} B_y, \\
 \ddot{y} &= -\frac{q}{M_i} E_y, \\
 \ddot{s} &= -\frac{q}{M_i} E_s + \frac{q}{M_i} \dot{x} B_y.
 \end{aligned} \quad (22)$$

The effect of fringing field has been taken into account using for B_y :

$$B_y(s) = B_{y0} \frac{1}{2} \left[1 + \cos\left(\pi \frac{s}{2g}\right) \right] \quad (23)$$

where g is the gap of the dipole and the negative (positive) sign refers to the beginning (end) of the dipole.

For the oscillating magnetic field of the insertion devices, (Wiggler), the real measured vector $B_y(s)$ was used. The reason is the non-uniform geometry of the alternating magnetic poles, for which the field is not easily reproducible by a mathematical function. In Fig. 4 the measured magnetic field $B_y(s)$ of a DAΦNE Wiggler and the horizontal beam centre co-ordinate X_c are reported vs. the longitudinal co-ordinate s .

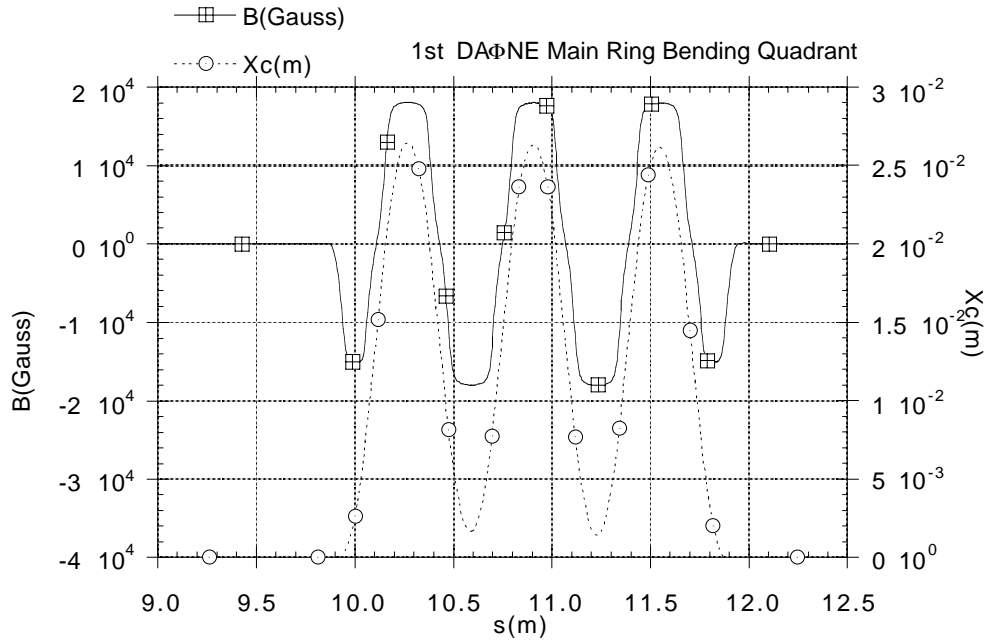


Figure 4. The plot shows the behaviour of the measured magnetic field in the first Wiggler of the DAΦNE Main Ring, and the correspondent electron beam centre co-ordinate X_c vs. the longitudinal one s . The zero line of the beam centre co-ordinate corresponds to the axis of the vacuum chamber.

The numerical integration of the ion motion equations has been performed using the integration subroutine of the NAG FORTRAN Libraries for stiff equations. The check on the stiffness was necessary because of the insertion of the discrete values of the measured Wiggler magnetic field vector instead of a continuous mathematical function.

VI. DC ION CLEARING AND RF BEAM SHAKING

The DC-clearing of the trapped ions is included in the ion motion equations by simply adding a constant component to the acceleration in the correspondent direction; e.g. :

$$\ddot{y} = -\frac{q}{m}(E_y - E_y^{DC}). \quad (24)$$

To evaluate the right value of the clearing electric field, inside the vacuum chamber, the Poisson equation with *Dirichlet boundary conditions* has been solved, (see C), for a suitable geometry for both Wiggler and dipole zones.

It happens quite often that the required DC voltage is too high compared to the electrode feasibility. In this case RF-shaking of the electron beam can help to reduce the needs of a high voltage [8]. In fact lower values for the DC “kick” are required around the maximum of the oscillating orbit of the ion. The beam shaking is included in the ion motion equations as a sinusoidal motion of the beam centre co-ordinate, around which the beam charge distributes and moves rigidly ; e.g.:

$$Y_c = Y_{c0} + f \cdot \sigma_y \cos(2\pi\tilde{\nu}t), \quad (25)$$

where $f = \tilde{A}/\sigma_y$, and $\tilde{\nu}$ belongs to the whole set of excited frequencies [9]:

$$\tilde{\nu} = \nu_{exc}^{RF} \pm n f_0, \quad (26)$$

where f_0 is the revolution frequency of the synchronous electron, and n takes the value that minimises the difference $\left| \tilde{\nu} - \frac{\omega_{H,V}}{2\pi} \right|$, where $\omega_{H,V}$ is the characteristic ion frequency .

VII. ION MOTION TRACKING RESULTS

The analysis of the ion motion has been performed first on the bending quadrants BQ of the main electron ring, (see App. D.1 and D.2). In Fig. 5 the potential $\Phi(X_c, Y_c, s)$ is shown in detail for the first BQ. The main interesting points are the minimum, (**a**), of the potential Φ , together with the dipole zones, (**1st** and **2nd** Bending Magnets), and the insertion device, (**Wiggler**). For the point **a**, corresponding to $s=13.64$ m, the evaluation of the average required DC clearing field [1], at full current, turns out to be:

$$E_{clearing} = \frac{Z_0 I}{2\pi(\sigma_x + \sigma_y)} \cong 173 \text{ kV/m}, \quad (27)$$

where $Z_0 = 1/(\epsilon_0 c)$ is the free space impedance and I the average current in the ring. To reach this value for the clearing field, in the vertical direction, with a square button shaped electrode and a vacuum chamber section $7.5 \times 5.3 \text{ cm}^2$, at least 14.4 kV need to be applied, (see App. C).

The tracked motion for the ion mass 44 is reported in Fig. 6 for the point **a**. The ionisation is considered to have taken place at the beam centre with negligible thermal velocity. The actual bunch structure of the beam leads to a lower value of the required $E_{clearing}$ in order to loose the trapped ions in a time $\tau \leq \tau_{drift}^{\max}$, (see Table A.1).

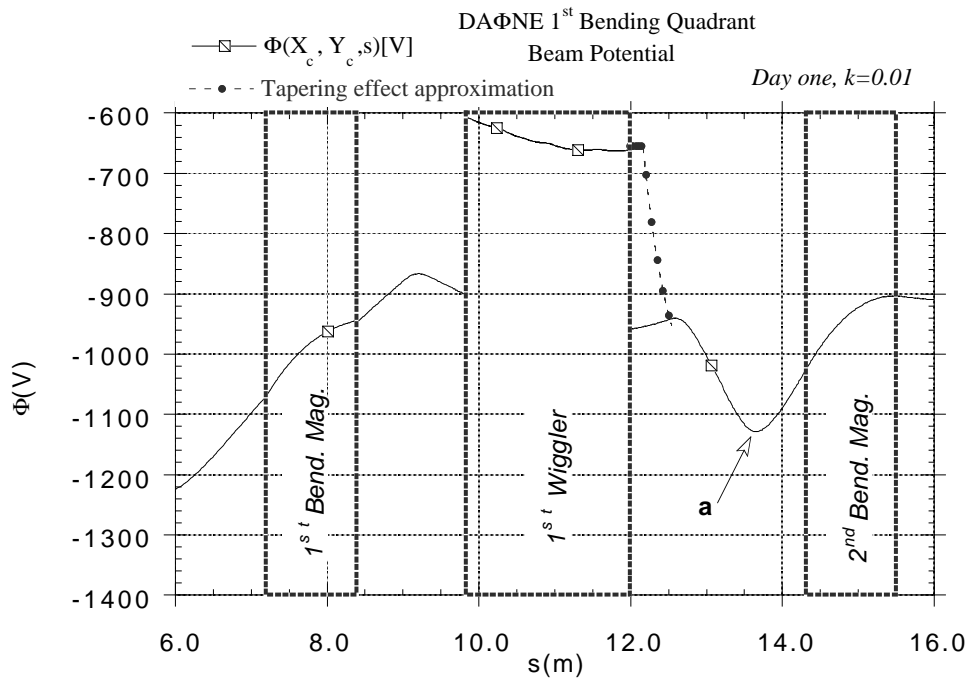


Figure 5. The potential $\Phi(x, X_c, y, Y_c, s)$ due to the electron beam, calculated in the beam centre position (see Sect. IV), is plotted vs. the longitudinal co-ordinate s for the first Bending Quadrant, BQ , of the DAΦNE Main Ring for electrons. The position of the lattice elements are also reported together with an estimate of the effect of the vacuum chamber tapering on the potential Φ . The “tapering curve” is actually a collection of discrete values of the potential Φ calculated for a vacuum chamber of infinite length and given, but variable in s , transverse dimensions.

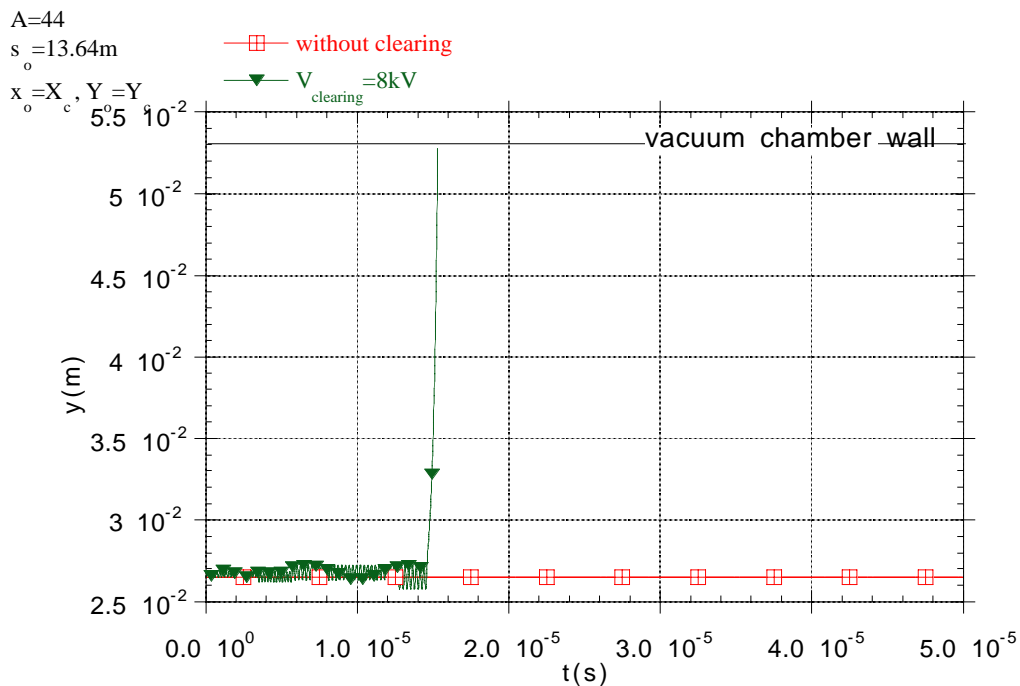


Figure 6. The transverse co-ordinate y of the tracked motion of the trapped mass 44 is reported vs. time, for the two cases with and without the vertical DC clearing field E_y .

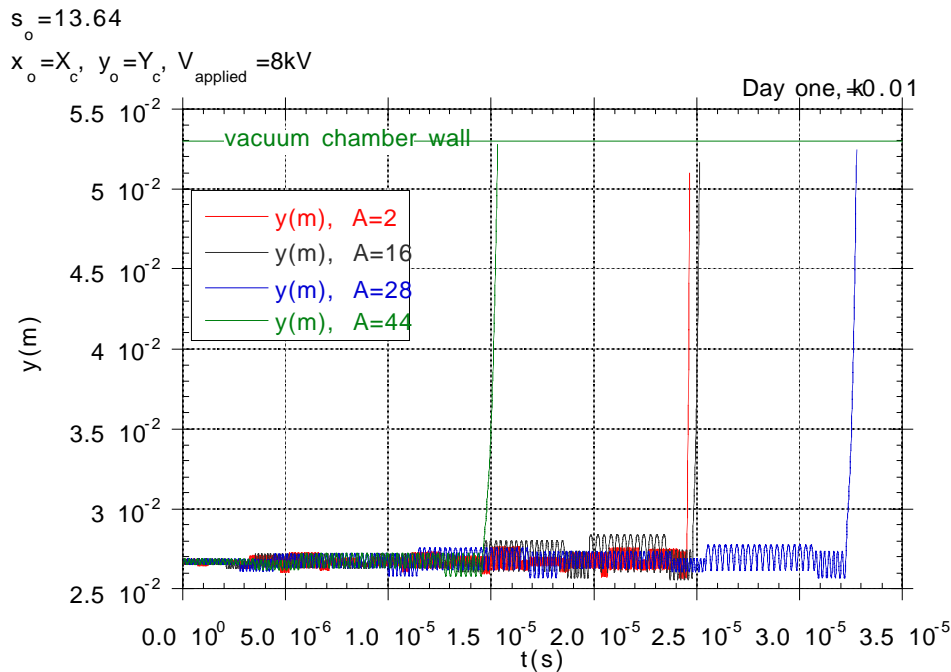


Figure 7. The transverse co-ordinate y of the ion tracked motion is shown for four different trapped masses, (corresponding to the four main residual gases present in the vacuum chamber), to check the effectiveness of the chosen value for the applied clearing voltage.

As far as the Wiggler is concerned, two accumulation points for trapped ions are found, i.e. the two minima of the oscillating magnetic field $B_y(s)$, see Fig. 4, corresponding to $s = 10.6m$ and $s = 11.2m$, respectively. Figure 8 refers to the first accumulation point; the effect of an applied clearing voltage of $\approx 1500\text{ V}$ is shown, together with the effect of the RF beam shaking and the tracked orbit of the unperturbed motion of the trapped ion.

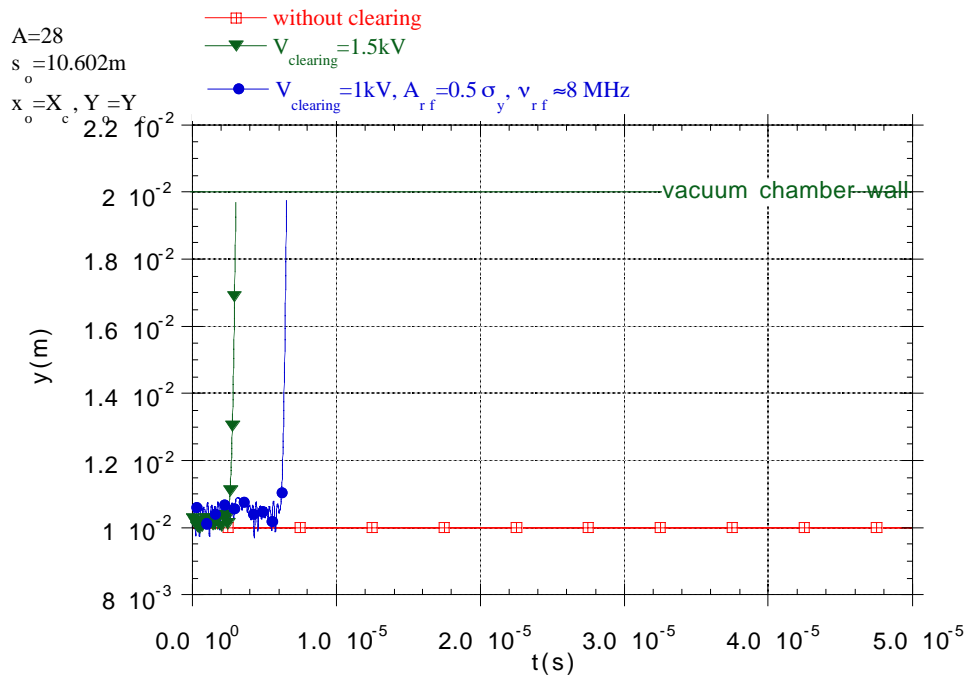


Figure 8. The transverse co-ordinate y of the tracked motion for the trapped mass 28 is plotted vs. time for three cases: with and without the vertical DC clearing field E_y , and with the effect of the RF electron beam shaking.

Other results for different points are collected in App. E. They refer to the 2nd Bending Quadrant that is almost the same of the first one but for the position of the deepest minimum of potential Φ and for the presence of another accumulation point for the ions close to the 4th Bending Magnet. The third and fourth Bending Quadrants are obtained by reflection of the first two BQ's due to the mirror symmetry of the DAΦNE Electron Ring lattice along the major axis, (see App. D.1).

VIII. CONCLUSIONS

The design of the clearing system for the DAΦNE electron ring bending quadrants is based on the results obtained solving numerically the motion equations for the ions trapped in the circulating electron beam. The boundary conditions are always taken to be very conservative, i.e. the residual gas atoms are considered to be ionised in the beam centre, with negligible thermal velocity, and, for the high luminosity requirements, the electron current is given its maximum value as the number of equidistantly filled bunches.

Moreover the considered value for the maximum tolerable vertical tune shift, induced by the ion trapping effect, is very low, even though it has to be considered as a hard task which can be relaxed under proper considerations and discussion on the tolerable detriments on the beam performances.

In this scenario DC clearing electrodes are needed in the potential well minima locations and also in those points where the Wiggler magnetic field takes its lowest values. Further the “mirror effect” due to the fringe field of the bending sections has been considered; [11,12], the location of the clearing electrodes has been optimized in order to cope also with this effect. Troubles arise from the practical point of view, since each DAΦNE Wiggler is actually a two meters long “closed box”, for there is no room for placing any feed-through between the magnetic pole expansions. The clearing electrode for the wiggler has then to be thought as a two meters long strip, biased at the first available place outside the first or the last magnetic pole. The other electrodes locations seem to be less hard since the length of the eventual strip should be around 20 cm. As far as the RF beam shaking is concerned it should be feasible to apply the proper oscillating component to the electrodes of the transverse feedback system for the electron beam. Similar considerations are to be applied also to the positron beam in order to make the two beams collide with the right phase at the two interaction points.

Appendix A :

“Calculation of the relevant parameters of the ion clearing system for the DAΦNE Electron Main Ring”

In order to estimate the neutralisation factor η , we must set an upper limit to the maximum tolerable linear tune shift $\delta Q_{H,V}$ due to the presence of the ion space charge. For rectangular gaussian beams we have that :

$$\frac{\frac{\partial F_x}{\partial x}}{\frac{\partial F_y}{\partial y}} = \frac{\sigma_y}{\sigma_x} < 1, \quad (\text{A.1})$$

therefore for flat beams, *i.e.* $\sigma_y \ll \sigma_x$, the vertical tune shift is the critical one. The chosen limit for DAΦNE is $\delta Q_y \leq 0.001$, and the analysis of the betatron functions has been limited to one half of the Main Ring due to its mirror symmetry .

For the neutralisation factor $\langle \eta \rangle$ we have[6]:

$$\langle \eta \rangle \equiv \frac{\Delta Q \cdot \gamma}{D \cdot A \cdot I_{beam}}, \quad (\text{A.2})$$

where :

γ = electron energy normalised to the electron energy at rest;

I_{beam} = beam current (A)

$$A = \left\langle \frac{\sqrt{\beta_y} (1 + K)}{\sqrt{K} (\sqrt{\beta_x} + \sqrt{K\beta_y})} \right\rangle,$$

$$D = \frac{r_e \cdot C}{\pi \cdot c \cdot e} (A^{-1})$$

with r_e = classical electron radius.

The DAΦNE project requirements for the beam lifetime limit the value of the mean pressure in the Main Rings of the collider to:

$$\langle P \rangle = 1 \times 10^{-9} \text{ Torr}, \quad (\text{CO related}) \quad (\text{A.3})$$

The gas load is mainly due to the synchrotron radiation induced gas desorption from the vacuum chamber walls. The measured percentage [7] of CO is about the 35% of the total photo-desorbed gas load (CO related). It means a partial pressure of

$$\bar{P}(\text{CO}) \approx 3.5 \times 10^{-10} \text{ Torr} \quad (\text{A.4})$$

and a gas density :

$$\bar{\rho}(\text{CO}) \approx 3.5 \times 10^{-10} \cdot 3.294 \times 10^{22} = 1.153 \times 10^{13} \text{ m}^{-3}, \text{ at } 20 \text{ }^\circ\text{C}. \quad (\text{A.5})$$

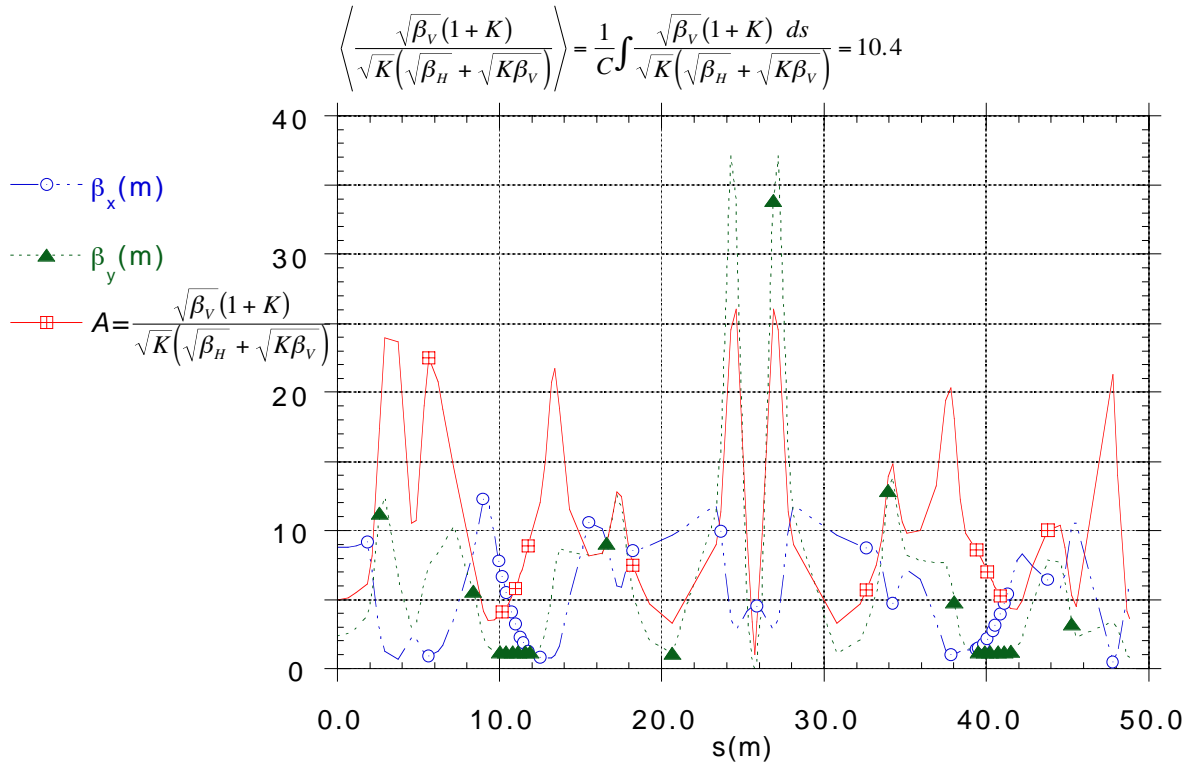


Figure A.1. The optical functions of half DAΦNE Man Ring are shown as function of the longitudinal coordinate s , starting from the half long straight section. The value of the quantity A is also reported.

Therefore:

$$\frac{1}{\tau_{prod.}(CO)} = c\sigma_p\bar{\rho} \cong 0.483s^{-1}, \quad (A.6)$$

where $\sigma_p^{CO} \cong 1.4 \times 10^{-18} cm^2$ [3].

The DAΦNE project provides three operating values for the beam current, i.e. three value sets of the neutralisation factor η , ($I=5.3 A$ with 120 bunches, $I=2.65 A$ with 60 bunches and $I=1.325 A$ with 30 bunches). The resulting values of τ_{drift}^{max} , for the two main residual gases, are then used to design the ion clearing system. In table A.1 the results for η and τ_{drift}^{max} are reported.

Table A.1. The results for the neutralisation factor η and the maximum drift time τ_{drift}^{max} of the trapped ions are reported for the two main residual gases present in the vacuum chamber and three different operating values of the DAΦNE electron beam current.

	η^{120b}	$\tau_{drift}^{120b}(s)$	η^{60b}	$\tau_{drift}^{60b}(s)$	η^{30b}	$\tau_{drift}^{30b}(s)$
H ₂	$\cong 1 \times 10^{-5}$	$\cong 4.2 \times 10^{-5}$	$\cong 2 \times 10^{-5}$	$\cong 8.4 \times 10^{-5}$	$\cong 4 \times 10^{-5}$	$\cong 1.7 \times 10^{-4}$
CO	” ”	$\cong 2 \times 10^{-5}$	” ”	$\cong 4.1 \times 10^{-5}$	” ”	$\cong 8.3 \times 10^{-5}$

Appendix B:

“Solution of the Poisson equation with *Dirichlet boundary conditions* for a rectangular box of infinite length”

Starting from the Poisson equation* :

$$\begin{cases} \nabla^2 \Phi = -4\pi\rho & \text{inside the vacuum chamber} \\ \Phi = 0 & \text{on the chamber walls (i.e. Dirichlet b.c.)} \end{cases} \quad (\text{B.1})$$

The definition of the Green's functions is:

$$\nabla'^2 G(\bar{x}, \bar{x}') = -4\pi\delta(\bar{x}, \bar{x}'), \quad (\text{B.2})$$

and by applying the Green's theorem to the potential Φ and the function $G(\bar{x}, \bar{x}')$ we can obtain:

$$\begin{aligned} \Phi(\bar{x}) = & \int_V \rho(\bar{x}') G(\bar{x}, \bar{x}') d^3x' + \\ & + \frac{1}{4\pi} \oint_S \left[G(\bar{x}, \bar{x}') \frac{\partial \Phi}{\partial n'} - \Phi(\bar{x}') \frac{\partial G(\bar{x}, \bar{x}')}{\partial n'} \right] da' \end{aligned} \quad (\text{B.3})$$

For the *Dirichlet boundary conditions* we impose:

$$G_D(\bar{x}, \bar{x}') = 0 \quad \text{for } \bar{x}' \in S. \quad (\text{B.4})$$

$$\rho(x, y) = \frac{\lambda}{2\pi\sigma_x\sigma_y} \cdot e^{-\left(\frac{(x-X_c)^2}{2\sigma_x^2} + \frac{(y-Y_c)^2}{2\sigma_y^2}\right)},$$

$$\lambda = \frac{N_e^{Tot} \cdot e}{C} = \text{linear charge density,}$$

x, y = horizontal and vertical transverse co-ordinates,

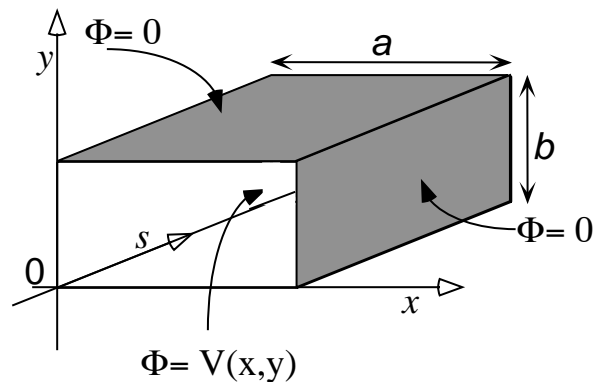
s = longitudinal co-ordinate of the motion of ions and electrons,

N_e^{Tot} = total number of electrons,

C = total circumference of the ring,

σ_x, σ_y = standard deviations of the electron distribution,

X_c, Y_c = beam centre transverse co-ordinates.



* C.G.S. units.

Furthermore, in our case :

$$\Phi = 0 \quad \text{for } \bar{x}' \in S \quad (\text{B.5})$$

so that:

$$\Phi(\bar{x}) = \int_V \rho(\bar{x}') G_D(\bar{x}, \bar{x}') d^3 x'. \quad (\text{B.6})$$

In the case of a uniform charge distribution along z , eq. (B.6) becomes

$$\Phi(\bar{r}) = \int_S \rho(\bar{r}') d\bar{r}' \cdot g(\bar{r}, \bar{r}'). \quad (\text{B.7})$$

For the $g(\bar{r}, \bar{r}')$ it holds:

$$\left(\frac{\partial^2}{\partial x^2} + \frac{\partial^2}{\partial y^2} \right) g(\bar{r}, \bar{r}') = -4\pi \delta(x - x') \delta(y - y'), \quad (\text{B.8})$$

and:

$$g(S, \bar{r}') = 0. \quad (\text{B.9})$$

The solution is found to be:

$$g(\bar{r}, \bar{r}') = \sum_{n,m=1}^{\infty} \frac{16}{\pi ab} \frac{\sin\left(\frac{n\pi x}{a}\right) \sin\left(\frac{n\pi x'}{a}\right) \sin\left(\frac{m\pi y}{b}\right) \sin\left(\frac{m\pi y'}{b}\right)}{\frac{n^2}{a^2} + \frac{m^2}{b^2}}, \quad (\text{B.10})$$

where a, b are the vacuum chamber cross section dimensions and which gives for the potential Φ :

$$\Phi(x, y) = \frac{16}{\pi ab} \sum_{n,m} \int_0^a dx' \int_0^b dy' \rho(x', y') \frac{\sin\left(\frac{n\pi x}{a}\right) \sin\left(\frac{n\pi x'}{a}\right) \sin\left(\frac{m\pi y}{b}\right) \sin\left(\frac{m\pi y'}{b}\right)}{\frac{n^2}{a^2} + \frac{m^2}{b^2}}. \quad (\text{B.11})$$

In our case $\sigma_x \ll a$ and $\sigma_y \ll b$ so we can replace the integration limits of (B.11) with $\pm\infty$, carry on the integration and obtain the solution:

$$\Phi(x, y) = \lambda \frac{16}{\pi ab} \sum_{n,m} \frac{\sin\left(\frac{n\pi x}{a}\right) \sin\left(\frac{n\pi X_c}{a}\right) \sin\left(\frac{m\pi y}{b}\right) \sin\left(\frac{m\pi Y_c}{b}\right)}{\frac{n^2}{a^2} + \frac{m^2}{b^2}} \cdot \exp\left[-\left(\frac{\pi^2 n^2 \sigma_x^2}{2a^2} + \frac{\pi^2 m^2 \sigma_y^2}{2b^2}\right)\right]. \quad (\text{B.12})$$

Appendix C:

“Solution of the Poisson Equation with Dirichlet b.c. for a circular box of infinite length” The approach is the same of Appendix A, (see equations B1-B6). For a uniform charge distribution along the z variable and with a vacuum chamber of circular cross section we can write:

$$\Phi(r, \theta) = \int_0^a r' dr' \int_0^{2\pi} d\theta' \rho(r', \theta') \sum_{m=-\infty}^{\infty} 2\pi g_m(r, r') e^{im(\theta-\theta')}. \quad (\text{C.1})$$

The Poisson equation is:

$$\frac{1}{r'} \partial_{r'} (r' \partial_{r'} g_m) - \frac{m^2}{r'^2} g_m = -\frac{2}{r} \delta(r - r'), \quad (\text{C.2})$$

i.e.:

$$\left[\frac{\partial^2}{\partial r'^2} + \frac{1}{r'} \frac{\partial}{\partial r'} - \frac{m^2}{r'^2} \right] g_m(r, r') = -\frac{2}{r} \delta(r - r'). \quad (\text{C.3})$$

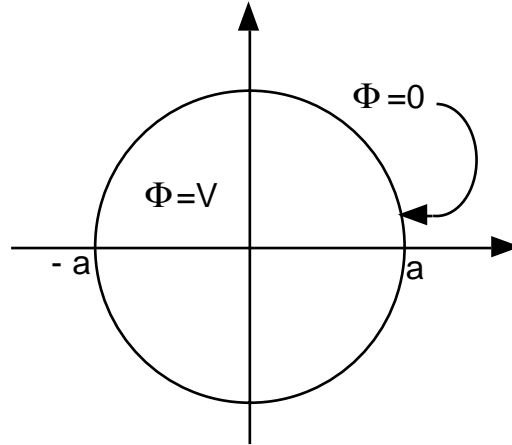


Figure C.1. Bi-dimensional case of circular box of infinite length where the external surface is kept at ground potential.

The solution of the above equation is :

$$\left\{ \begin{array}{l} g_0(r, r') = -2 \ln \left(\frac{r_{>}}{a} \right) \\ g_m(r, r') = \frac{1}{m} \left[\left(\frac{r_{<}}{r_{>}} \right) - \frac{(rr')^m}{a^{2m}} \right] \end{array} \right\}, \quad \text{where: } r_{>} = \begin{cases} r, & \text{if } r > r' \\ r', & \text{if } r' > r \end{cases} \quad (\text{C.4})$$

For the charge density $\rho(r', \theta')$ we have :

$$\rho(r', \theta') = \frac{\lambda}{2\pi\sigma_x\sigma_y} \exp\left\{\frac{r'^2}{2} \left[\frac{1}{2\sigma_x^2} + \frac{1}{2\sigma_y^2} + \frac{\cos 2\theta'}{2} \left(\frac{1}{\sigma_x^2} - \frac{1}{\sigma_y^2} \right) \right]\right\}, \quad (\text{C.5})$$

that leads to :

$$\begin{aligned} \Phi(r, \theta) = \frac{2}{\sigma_x\sigma_y} \int_0^a r' dr' \exp\left[-\frac{r'^2}{4} \left(\frac{1}{\sigma_x^2} + \frac{1}{\sigma_y^2} \right)\right] \cdot \left\{ -\ln\left(\frac{r_>}{a}\right) I_0\left(\frac{r'^2}{4} \left(\frac{1}{\sigma_x^2} - \frac{1}{\sigma_y^2} \right)\right) + \right. \\ \left. + \sum_{l=1}^{\infty} \frac{(-1)^l}{2l} I_l\left(\frac{r'^2}{4} \left(\frac{1}{\sigma_x^2} - \frac{1}{\sigma_y^2} \right)\right) \cdot \cos 2l\theta \cdot \left[\frac{r_{<}^{2l}}{r_{>}^{2l}} - \frac{(rr')^{2l}}{a^{4l}} \right] \right\}. \end{aligned} \quad (\text{C.6})$$

For $r = 0$, $r_{<} = r$ and $r_{>} = r'$ we obtain:

$$\Phi(0) = -\frac{2\lambda}{\sigma_x\sigma_y} \int_0^a dr' r' \exp\left[\frac{r'^2}{4} \left(\frac{1}{\sigma_x^2} + \frac{1}{\sigma_y^2} \right)\right] \ln\left(\frac{r'}{a}\right) I_0\left[\frac{r'^2}{4} \left(\frac{1}{\sigma_x^2} - \frac{1}{\sigma_y^2} \right)\right]. \quad (\text{C.7})$$

Appendix D:

“Calculation of the Electric Field due to a Clearing Electrode for a rectangular box of infinite length”

In order to evaluate the behaviour of electric field due to a DC biased electrode we can consider the case shown in Fig. D.1.: a rectangular conductive box with three sides at ground potential and the fourth with a strip of length Δ at the potential $\Phi=V$.

The definition of the Green’s function in the two-dimensional case is* :

$$\nabla^2 G(x, x', y, y') = -\delta(x - x')(y - y') \tag{D.1}$$

For the delta function we can write** :

$$\delta(x - x') = \frac{1}{2a} \sum_{n=-\infty}^{\infty} e^{\frac{im\pi}{a}(x-x')} \tag{D.2}$$

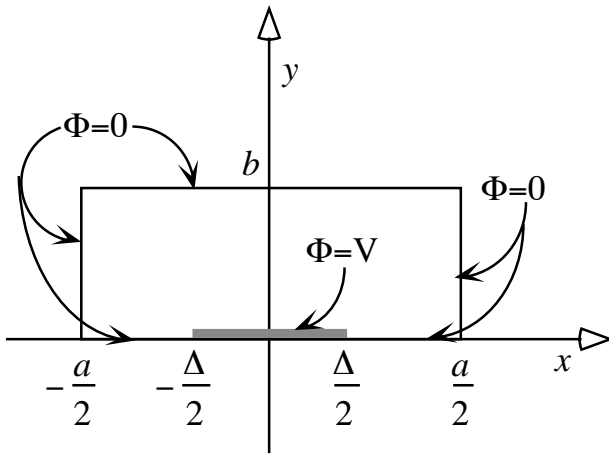


Figure D.1. Bi-dimensional case of a rectangular box with three sides at ground potential and the fourth centrally biased at $\Phi=V$ for a total length Δ .

and for our Green function :

* M.K.S. units.

** It’s always possible to expand a function $f(x)$ as a series of orthonormal functions. The generic function $f(x)$ may be expanded between $-\pi, \pi$ as:

$$f(x) = \sum_{m=-\infty}^{\infty} f_m e^{-imx}$$

where:

$$f_m = \frac{1}{2\pi} \int_{-\pi}^{\pi} f(x) e^{imx} dx.$$

Therefore:

$$f(x) = \int_{-\pi}^{\pi} f(y) \cdot \left[\frac{1}{2\pi} \sum_{m=-\infty}^{\infty} e^{im(x-y)} \right] dy$$

and for the delta function it holds :

$$\delta(x - x') = \frac{1}{2\pi} \sum_{m=-\infty}^{\infty} e^{im(x-x')}.$$

In our case $|x| \leq \frac{a}{2}$ and $|x'| \leq \frac{a}{2}$ so $|x - x'| \leq a$, and the representation for the delta-function is:

$$\delta(x - x') = \frac{1}{2a} \sum_{m=-\infty}^{\infty} e^{\frac{im\pi}{a}(x-x')}$$

$$\nabla^2 G = -\delta(y - y') \cdot \frac{1}{2a} \sum_{m=-\infty}^{\infty} e^{\frac{im\pi}{a}(x-x')}. \quad (\text{D.3})$$

We are looking for a solution like:

$$G = \frac{1}{2a} \sum_{m=-\infty}^{\infty} g_m(y, y') e^{\frac{im\pi}{a}(x-x')}; \quad (\text{D.4})$$

where g_m satisfies:

$$\left(\frac{\partial^2}{\partial y^2} - \frac{m^2 \pi^2}{a^2} \right) g_m = -\delta(y - y'). \quad (\text{D.5})$$

Therefore for $y < y'$:

$$g_m(y, y') = c_1(y') e^{-\frac{m\pi}{a}y} + c_2(y') e^{\frac{m\pi}{a}y}, \quad (\text{D.6})$$

while for $y > y'$:

$$g_m(y, y') = d_1(y') e^{-\frac{m\pi}{a}y} + d_2(y') e^{\frac{m\pi}{a}y}. \quad (\text{D.7})$$

With the help of the equation D.5 and the boundary conditions:

$$\begin{cases} g_m(0, y') = 0 \\ g_m(b, y') = 0 \end{cases} \quad (\text{D.8})$$

we obtain for $y < y'$:

$$g_m(y, y') = \frac{a}{m\pi} \left\{ \frac{\sinh\left[\frac{m\pi}{a}(b - y')\right]}{\sinh\left(\frac{m\pi}{a}b\right)} \sinh\left(\frac{m\pi}{a}y\right) \right\}, \quad (\text{D.9})$$

and for $y > y'$:

$$g_m(y, y') = \frac{a}{m\pi} \left\{ \frac{\sinh\left[\frac{m\pi}{a}(b - y)\right]}{\sinh\left(\frac{m\pi}{a}b\right)} \sinh\left(\frac{m\pi}{a}y'\right) \right\}. \quad (\text{D.10})$$

Therefore our Green function will be:

$$G(y, y') = g_0(y, y') + \frac{1}{2a} \sum_{m=1}^{\infty} g_m(y, y') \cdot \left[2 \left[\cos\left(\frac{m\pi}{a} x\right) \cos\left(\frac{m\pi}{a} x'\right) + \sin\left(\frac{m\pi}{a} x\right) \sin\left(\frac{m\pi}{a} x'\right) \right] \right], \quad (D.11)$$

with:

$$\begin{cases} g_0(y, y') = \frac{y(b-y')}{2ab} & \text{for } y < y' \\ g_0(y, y') = \frac{y'(b-y)}{2ab} & \text{for } y' < y \end{cases}. \quad (D.12)$$

The *Green theorem* states that:

$$\int (G \nabla^2 \Phi - \Phi \nabla^2 G) d^3 x' = \int dS' \left(G \frac{\partial \Phi}{\partial n'} - \Phi \frac{\partial G}{\partial n'} \right); \quad (D.13)$$

from which we obtain :

$$\int_V \left[-\Phi(\bar{x}') \delta(\bar{x} - \bar{x}') + G(\bar{x}, \bar{x}') \frac{\rho(\bar{x}')}{\epsilon_0} \right] d^3 x' = \oint_S \left[\Phi \frac{\partial G}{\partial n'} - G \frac{\partial \Phi}{\partial n'} \right] da'. \quad (D.14)$$

Since in our case $\rho(\bar{x}') = 0$ inside the volume V , and $G(S, \bar{x}') = 0$, we obtain:

$$\Phi(x, y) = - \int_S \Phi \frac{\partial G}{\partial n'} da' = V_{appl.} \int_{-\Delta/2}^{\Delta/2} dx' \frac{\partial G}{\partial y'} \Big|_{y'=0}. \quad (D.15)$$

Therefore:

$$\frac{\Phi(x, y)}{V_{appl.}} = \frac{(b-y) \cdot \Delta}{2ab} + \sum_{m=1}^{\infty} \frac{\sinh\left(\frac{m\pi}{a}(b-y)\right)}{\sinh\left(\frac{m\pi}{a}b\right)} \cos\left(\frac{m\pi}{a}x\right) \cdot \frac{1}{a} \int_{-\frac{\Delta}{2}}^{\frac{\Delta}{2}} dx' \cos\left(\frac{m\pi}{a}x'\right). \quad (D.16)$$

Carrying out the integration we obtain:

$$\frac{\Phi(x, y)}{V_{appl.}} = \frac{(b-y) \cdot \Delta}{2ab} + \sum_{m=1}^{\infty} \frac{2}{m\pi} \sin\left(\frac{m\pi}{2a} \Delta\right) \cos\left(\frac{m\pi}{a} x\right) \frac{\sinh\left(\frac{m\pi}{a}(b-y)\right)}{\sinh\left(\frac{m\pi}{a} b\right)}. \quad (D.17)$$

The value of the vertical component of the electric field, at the beam centre, is:

$$\frac{E_y(x, y)}{V_{appl.}} = -\frac{\partial \Phi(x, y)}{\partial y} = \frac{\Delta}{2ab} + \frac{2}{a} \sum_{m=1}^{\infty} \sin\left(\frac{m\pi \Delta}{2a}\right) \cos\left(\frac{m\pi x}{a}\right) \frac{\cosh\left[\frac{m\pi}{a}(b-y)\right]}{\sinh\left(\frac{m\pi b}{a}\right)}. \quad (D.18)$$

In Fig. D.2. the behaviour of E_y , at the beam centre, vs. the Clearing Electrode width is reported; the considered vacuum chamber cross section has dimensions $a=7.5\text{cm}$, $b=5.3\text{cm}$. In Fig. D.3. and D.4 the electric field E_y vs. the transverse co-ordinate is shown.

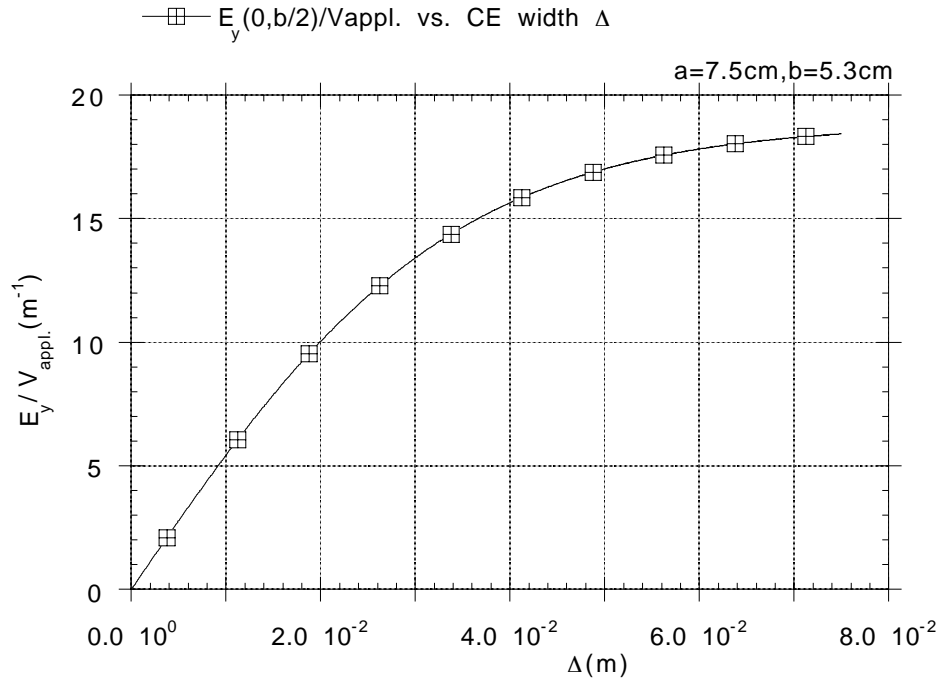


Figure D.2. The behaviour of the vertical component of electric field due to the Clearing Electrode CE, at $x=0$, $y=b/2$, normalised to the applied voltage $V_{appl.}$, vs. the electrode width Δ .

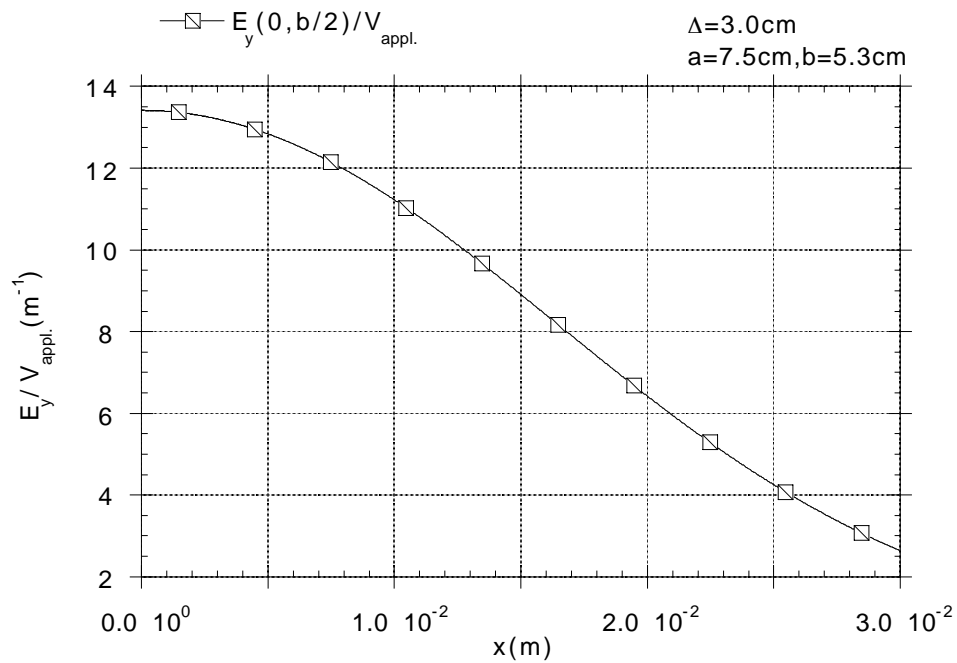


Figure D.3. The behaviour of the vertical component of electric field due to the Clearing Electrode CE, normalised to the applied voltage $V_{\text{appl.}}$, for an electrode width Δ , at $y=b/2$, vs. the x co-ordinate. (Bending Magnet zone)

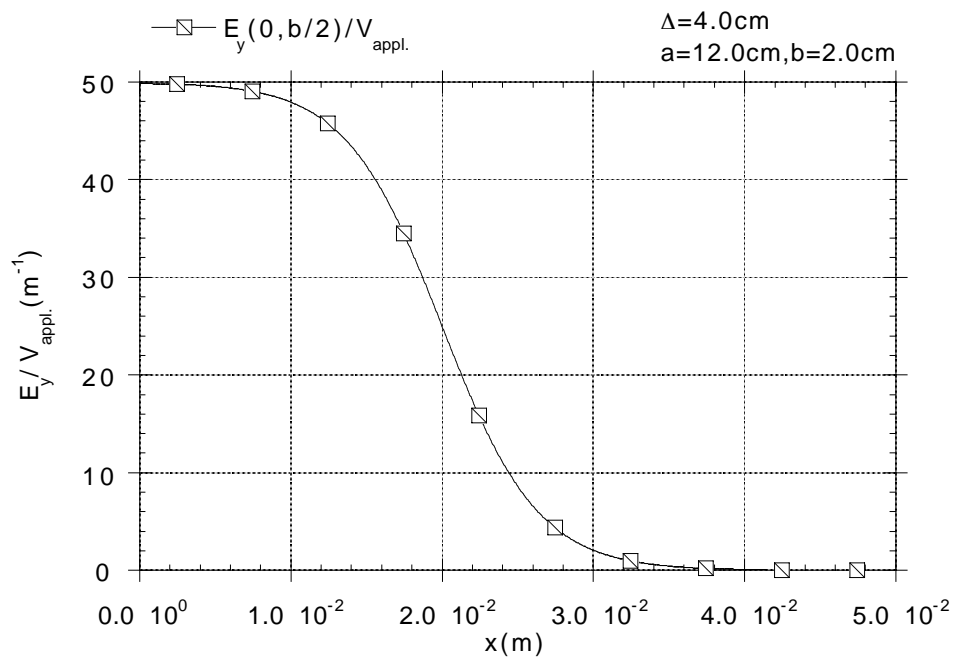


Figure D.4. The behaviour of the vertical component of electric field due to the Clearing Electrode CE, normalised to the applied voltage $V_{\text{appl.}}$, for an electrode width Δ , at $y=b/2$, vs. the x co-ordinate. (Wiggler)

Appendix E:

“Calculation of the Electric Field due to a Clearing electrode for a circular box of infinite length”

Following the notation of Appendix C.1, in this case we have for the potential only the contribution from the surface, (see eq. 16, p. 6)* :

$$\begin{aligned} \Phi(r, \theta) &= -\frac{1}{4\pi} \int_S da' \left(-V \frac{\partial G}{\partial r'} \right) = \\ &= V \int_{-\frac{\hat{\theta}}{2}}^{\frac{\hat{\theta}}{2}} \frac{a}{4\pi} d\theta' \frac{\partial}{\partial r'} \left\{ g_0(r, r') + 2 \sum_{m=1}^{\infty} \cos[m(\theta - \theta')] g_m(r, r') \right\} \Big|_{r'=a} \end{aligned} \quad (E.1)$$

Inserting in the above equation the solution C.4, we obtain:

$$\begin{aligned} \Phi(r, \theta) &= -\frac{V}{\pi} \sum_{m=1}^{\infty} \frac{r^m}{a^m} \int_{-\frac{\hat{\theta}}{2}}^{\frac{\hat{\theta}}{2}} d\theta' \cos[m(\theta - \theta')] = \\ &= -\frac{2V}{\pi} \sum_{m=1}^{\infty} \frac{r^m}{a^m} \frac{1}{m} \sin\left(\frac{m\hat{\theta}}{2}\right) \cos(m\theta) \end{aligned} \quad (E.2)$$

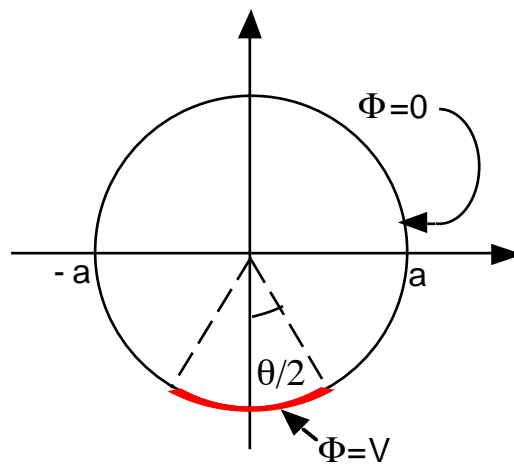


Figure E.1. Bi-dimensional case of circular box of infinite length where the external surface is kept at ground potential except for an arc of aperture θ .

* C.G.S. units.

The electrical field is given by:

$$\begin{aligned} \vec{E} &= -\frac{\partial\Phi}{\partial r}\vec{r} - \frac{1}{r}\frac{\partial\Phi}{\partial\theta}\vec{\theta} = \\ &= \frac{2V}{a\pi} \sum_{m=1}^{\infty} \sin\left(\frac{m\hat{\theta}}{2}\right) \frac{r^{m-1}}{a^{m-1}} \left[\cos(m\theta)\vec{r} - \sin(m\theta)\vec{\theta} \right] \end{aligned} \quad (\text{E.3})$$

Expressing \vec{r} and $\vec{\theta}$ as :

$$\begin{aligned} \vec{r} &= \cos\theta\vec{x} + \sin\theta\vec{y} \\ \vec{\theta} &= -\sin\theta\vec{x} + \cos\theta\vec{y} \end{aligned} \quad (\text{E.4})$$

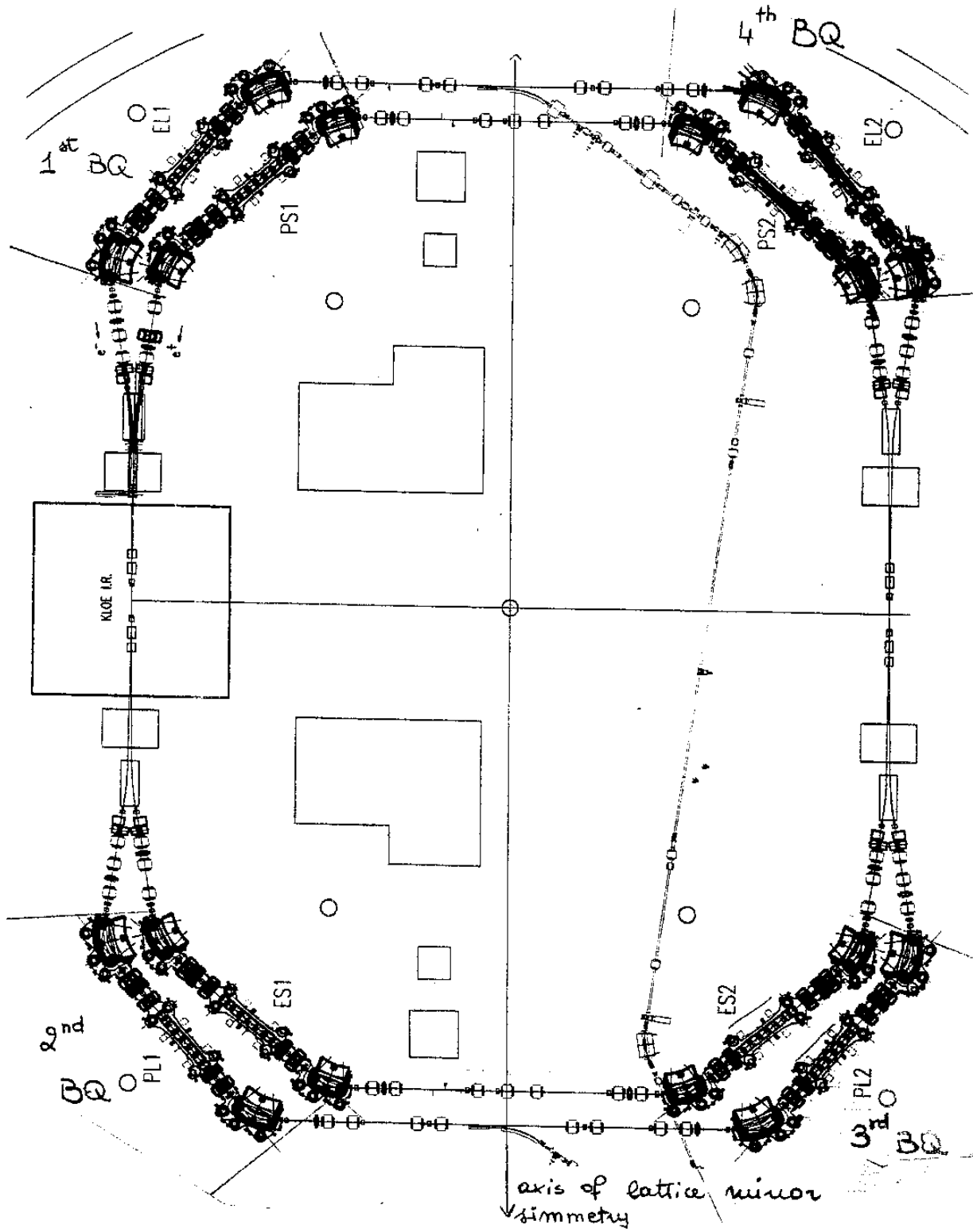
we can write the equation E.3 as:

$$\frac{\vec{E}}{V} = \frac{2}{a\pi} \sum_{m=1}^{\infty} \sin\left(\frac{m\hat{\theta}}{2}\right) \frac{r^{m-1}}{a^{m-1}} \left\{ \cos[(m-1)\theta]\vec{x} - \sin[(m-1)\theta]\vec{y} \right\}; \quad (\text{E.5})$$

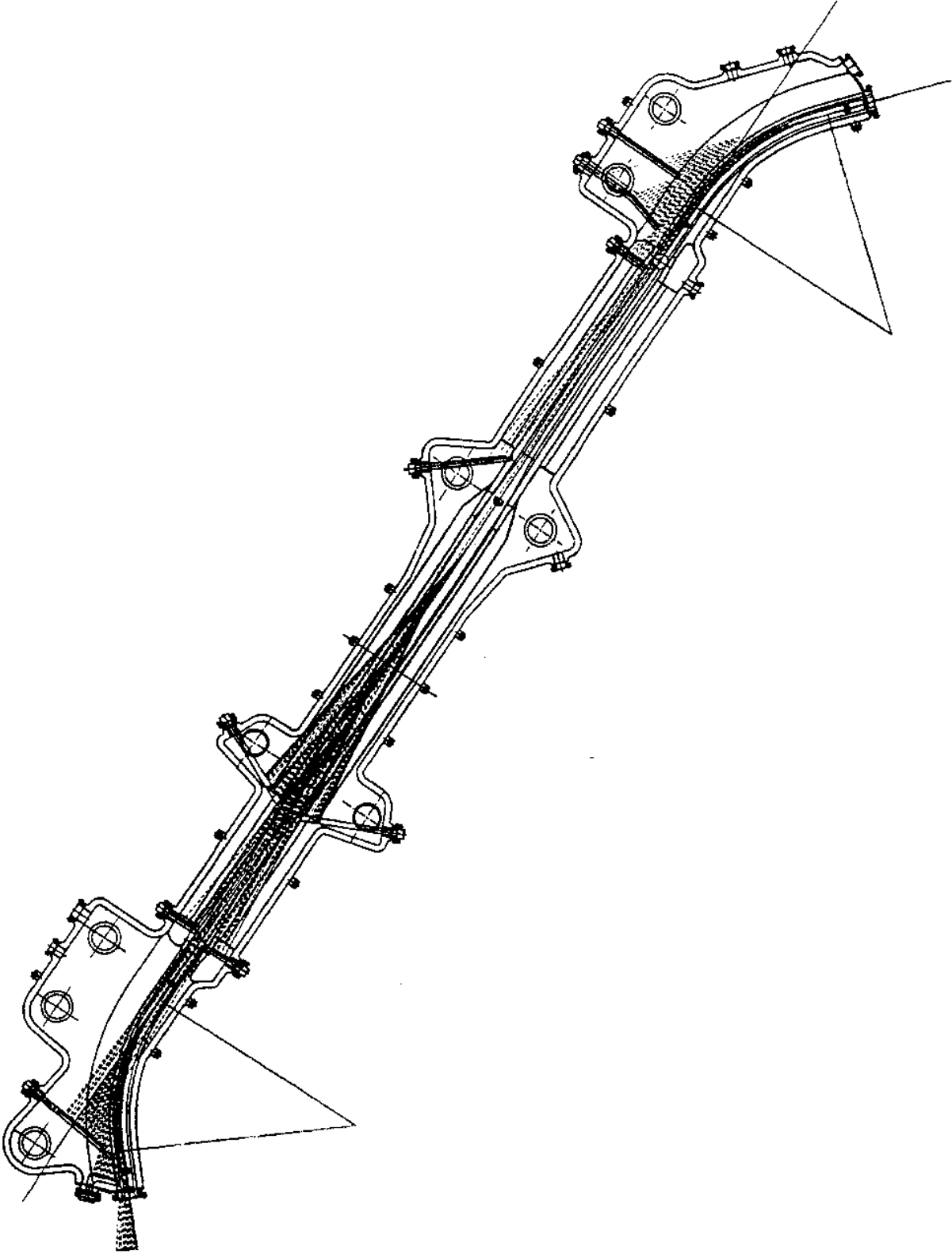
and for $r = 0$ we obtain:

$$\frac{E}{V} = \frac{2}{a\pi} \sin\left(\frac{\hat{\theta}}{2}\right)$$

Appendix F.1 :
"DAΦNE Electron Main Ring Layout"



Appendix F.2 :
“DAΦNE First Bending Quadrant Layout”



Appendix G :

“Other results of tracking for trapped ions in the second Bending Quadrant of DAΦNE Electron Main ring”

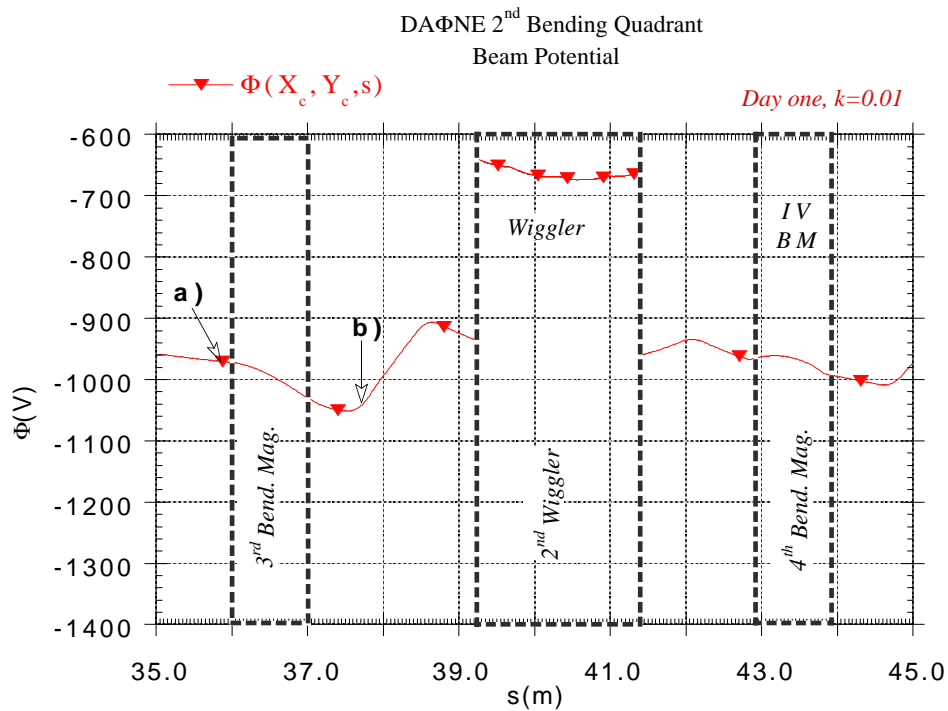


Figure E.1. The potential $\Phi(x, X_c, y, Y_c, s)$ due to the electron beam, calculated in the beam centre position (see Sect. IV), plotted vs. the longitudinal co-ordinate s for the second Bending Quadrant, BQ , of the DAΦNE Main Ring for electrons.

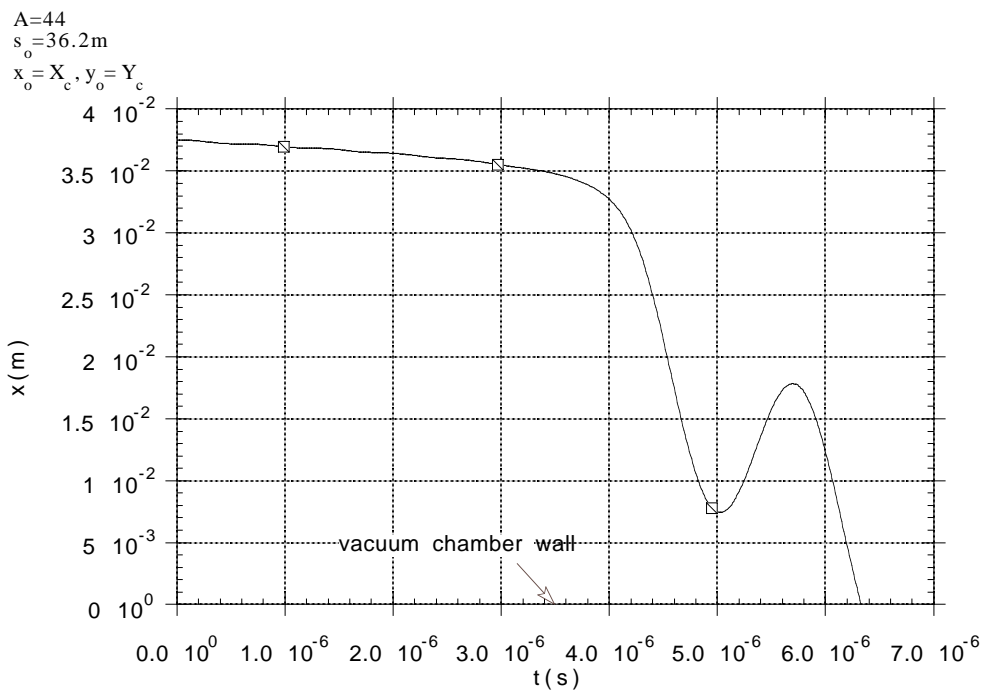


Figure E.2. The transverse co-ordinate x of the tracked orbit of a mass 44 ionised in the point **a**).

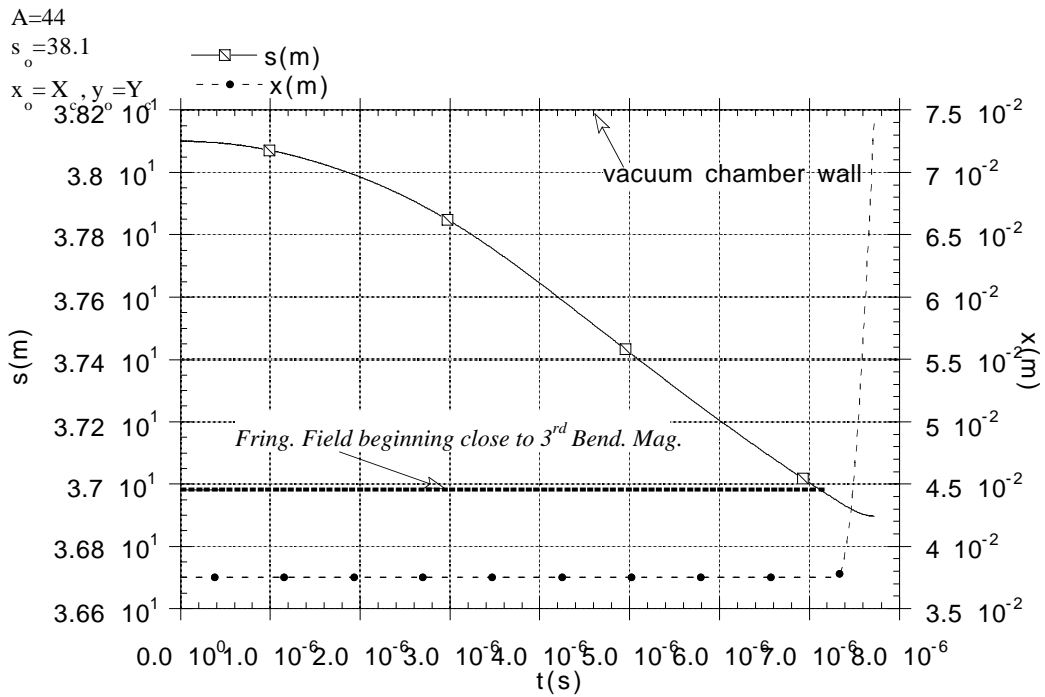


Figure E.3. The transverse co-ordinate x of the tracked orbit of a mass 44 ionised in the point **b**). The fringing field of the third dipole is effective in removing the trapped ion coupling the longitudinal speed v_s with the transverse one v_x .

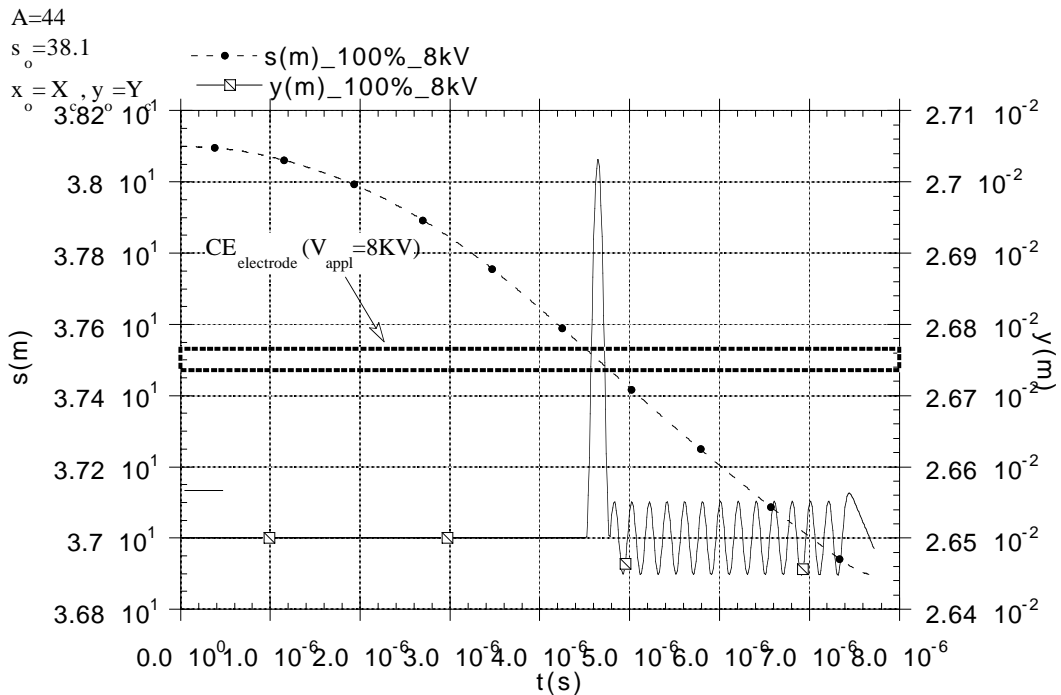


Figure E.4. The transverse co-ordinate y of the tracked orbit of a mass 44 ionised in the point **b**). The effect of a clearing electrode, (4 cm long), centred in $s=37.5$ m is shown ; it is not effective in removing the ion in the vertical direction.

REFERENCES

- [1] C.J. Bocchetta, A. Wrulich, Nucl. Inst.. & Met. A278 (1989), pp.807-817.
- [2] T. Kasuga, H. Yonehara, T. Kinoshita, M. Hasumoto, Jap. Jou. Appl. Phys. vol. 24, no. 9, (1985), pp. 1212-1217.
- [3] R. D. Kohaupt, DESY H1-71/2, Dec. 1971.
- [4] M.Q. Barton, Nucl. Inst.. & Met. A243 (1986), pp. 278-280.
- [5] M. Bassetti, G.A. Erskine, CERN-ISR-TH/80-06.
- [6] M. Sands, SLAC-121, UC-28 (ACC), Nov. 1970.
- [7] C. Foerster, H. Halama, C.Vaccarezza, submitted to Jou. Vac. Sci.&Techn.
- [8] A. Poncet ,“Frontiers of Particle Beams: Intensity Limitations” Proceedings of a Topical Course, p. 488-508, 1992, Springer-Verlag, Berlin, Germany.
- [9] M. Serio, CAS (CERN 91-04), p. 136-60.
- [10] Y. Miyahara, K. Takayama, G. Horikoshi, Nucl. Inst.. & Met. A270 (1988), pp.217-225.
- [11] D. Sagan, Nucl. Inst.. & Met. A307 (1991), pp.171-178.